INTERNATIONAL JOURNAL FOR NUMERICAL METHODS IN FLUIDS
Int. J. Numer. Meth. Fluids 2009; **59**:1389–1409
Published online 17 July 2008 in Wiley InterScience (www.interscience.wiley.com). DOI: 10.1002/fld.1879

A practical implementation of high-order RKDG models for the 1D open-channel flow equations

Georges Kesserwani[1, 2, *, †], Robert Mosé[1], José Vazquez[1] and Abdellah Ghenaim[2]

[1]*U.P.R. Systèmes Hydrauliques Urbains, Ecole Nationale du Génie de l'Eau et de l'Environnement de Strasbourg, 1 quai Koch -BP 61039, 67070 Strasbourg Cedex, France*
[2]*Institut National des Sciences Appliquées, 24 boulevard de la Victoire, 67084 Strasbourg Cedex, France*

SUMMARY

This paper comprises an implementation of a fourth-order Runge–Kutta discontinuous Galerkin (RKDG4) scheme for computing the open-channel flow equations. The main features of the proposed methodology are simplicity and easiness in the implementation, which may be of possible interest to water resources numerical modellers. A version of the RKDG4 is blended with the Roe Riemann solver, an adaptive high-order slope limiting procedure, and high-order source terms approximations. A comparison of the performance of the proposed method with lower-order RKDG models is performed showing a benefit of considering the RKDG4 model. The scheme is applied to computerize the Saint Venant system by considering benchmark tests that have exact solutions. Finally, numerical results are illustrated discussing the performance of the proposed high-order model. Copyright © 2008 John Wiley & Sons, Ltd.

Received 7 April 2008; Revised 4 June 2008; Accepted 5 June 2008

KEY WORDS: high order; RKDG; adaptive limiting; 1D; Saint Venant; source terms

1. INTRODUCTION

Over the past few decades, considerable attentions have been paid to the development of numerical algorithms capable of achieving optimal performance for solving flow problems in computational fluid dynamics [1–4]. In the context of shallow water dynamics, finite difference, finite volume (FV), and finite element (FE) numerics have become very popular. Most discrete formulations for the set of shallow water equations [5, 6] are reflections of high-resolution schemes originally devised to solve high-speed compressible flows and have been successfully employed in the simulation of flows including the presence of shock waves, such as breaking dams or hydraulic jumps, almost

*Correspondence to: Georges Kesserwani, U.P.R. Systèmes Hydrauliques Urbains, Ecole Nationale du Génie de l'Eau et de l'Environnement de Strasbourg, 1 quai Koch -BP 61039, 67070 Strasbourg Cedex, France.
†E-mail: georges.kesserwani@engees.u-strasbg.fr

invariably neglecting viscous and turbulent effects. For an informal overview, we refer the reader to the recent papers of van Leer [7] and Toro and García-Navarro [8].

In recent years, research on reliable numerical models, of first or higher order, for solving hyperbolic partial differential equations (PDEs) is still growing and becoming difficult to follow. Burguete and García-Navarro [9] pioneered a new approach for constructing high-resolution total variation diminishing (TVD) schemes through considering applications to shallow water flows. Hsu and Yeh [10] built an iterative explicit scheme suitable for solving 1D unsteady open-channel flow problems based on the Saint Venant equations. Delis and Katsaounis [11] incorporated the source term vector into the IMEX implicit–explicit relaxation model. Črnjarić-Žic *et al.* [12] extended the finite volume weighted essentially non-oscillatory (WENO) schemes and central WENO schemes, by particularly considering open-channel flow benchmarks. Liang *et al.* [13] put the focus on a high-resolution numerical model of shallow flow hydrodynamics based on dynamically adaptive quadtree grids. Crossely and Wright [14] presented local time stepping strategies to simulate 1D unsteady water flows. Murillo *et al.* [15] empowered an extension of the first-order explicit upwind scheme to Courant–Friedrichs–Lewy (CFL) [16] values greater than 1. Very recently, Mohammadian *et al.* [17] carried forward an extension to the non-conservative method of characteristics (MOC). By using a proper interpolation function, the MOC scheme is rendered conservative and can handle challenging tests for the 1D open-channel flow (dam-break type, transcritical flows). Vignoli *et al.* [18] enabled the construction of Arbitrary (very) high-order schemes using DERivatives (ADER) schemes for solving the 1D shallow water equations with variable bed elevation. The cornerstone of this recent approach is the solution of the derivative Riemann problem [19], which is a generalization to the Riemann problem firstly introduced by Godunov [3, 20].

Very high-order methods are the next generation of numerical schemes to be used in shallow water type flow and related problems. Classically, the concept of high-order methods is most frequently used in the literature to formally reference second-order methods [1–3, 9]. However, the development of higher than second-order methods has a widespread applicability. Various numerical modellers have reported that first-order and even second-order upwind schemes, despite providing excellent results in the case of discontinuous flow, exhibit excessive numerical dissipation when applied to more general flows (not necessary including a bore propagation). On the other hand, smooth regions of the spatial domain may be most economically approximated using relatively high-order methods. It is broadly recognized that the higher the accuracy order of a numerical model, the lesser the number of computational cells required to achieve a desired fixed level of accuracy [21].

The first-order Godunov [20] and Lax-Friedrich [22] schemes are, respectively, the forerunners of the large class of upwind and central high-resolution FV schemes. However, a cell average of a solution in a cell contains very little information. In order to obtain higher-order accuracy, neighboring cells' averages must be used to reconstruct an approximate polynomial solution in each cell. The development of high-order Godunov-type [7, 8] FV methods, because of the absence of an underlying spatial approximation framework, which stems from the inherent piecewise constant representation, is certainly the most challenging algorithmic issue for researchers, since the construction of high-order polynomials requires the evaluations of high-order derivatives of the field variables from scattered pointwise information. As a result, most traditional TVD [1–3, 9, 11, 13, 14, 23, 24] schemes are at best second-order where a reconstruction of fluxes and gradients is frequently required. We also mention here the notable example of the high-resolution FV upwind flux-corrected transport, monotone upstream-centered schemes for conservation laws,

DOI: 10.1002/fld

piecewise parabolic method, essentially non-oscillatory, and WENO [23, 25–33] and this list is far from being complete.

Unlike FV models, the intrinsic advantage of a discontinuous Galerkin (DG) spatial discretization approach [34, 35] lies in their locality. A DG approach stores and evolves every polynomial coefficient in a cell over time. Therefore, there is no need to use information in non-local cells to achieve high-order accuracy. In addition, the DG approach conserves the Godunov-type methods' features through the use of the Riemann problem [2, 36–38] solution (in the computation of the intercell flux) and the involvement of slope limiters [28, 32, 39, 40] to avoid spurious oscillations in the vicinity of strong shocks. In point of fact, the first-order DG method boils down to the original Godunov upwind scheme [20]. Moreover, high-order DG approximations can deliver faster convergence rates than high-order FV reconstructions and, hence, have the advantage of achieving the same error magnitude as FV methods with less CPU time cost [21, 41]. Nonetheless, the price one has to pay is the memory requirements, because the more we increase the order of a DG approximation, the more the number of degrees of freedoms, to compute an approximate solution, will locally increase.

The basic idea of Cockburn *et al.* [34, 35] was a simple yet elegant one. The investigators used a DG discretization in space along with the TVD preserving Runge–Kutta (RK) time integration from Shu and Osher [31] to arrive at a methodology called Runge–Kutta discontinuous Galerkin (RKDG), which since its introduction by Reed and Hill [42] has experienced a vigorous development in wide fields of hyperbolic PDEs [43]. Some of the illuminating profits of dealing with the RKDG technique are (i) it increases the degree of approximating polynomial locally and thus can readily support h- and p-adaptation strategies [44] and (ii) it communicates each element data with its immediate neighbors only, regardless of the order of accuracy, thus allowing an easiness in the external boundary condition treatment as well as to efficient parallel implementations [39]. The list of new developments in DG methods is growing and far from being complete, we mention here the remarkable work of Liu *et al.* [45] who introduced a central type [24, 46] DG scheme that avoids solving the Riemann problems across boundaries and the work of Dumbser and Munz [47, 48] who built an ADER approach using DG approximations for a very high-order model.

Primordial applications of the DG method to the conservative form of the Saint Venant system [43, 49] were implemented with the Harten Lax and van Leer (HLL) Riemann solver [38]. Recently, Xing and Shu [50] have extended high-order FV-WENO and FE-RKDG schemes, both implemented with the simplest and inexpensive local Lax Friedrich (LLF) [22] Riemann solver, to particularly solve the shallow water equations. However, this Riemann solver is an ideal choice to be employed within RKDG methods for simulating shallow water flows when the model merely considers frictionless and horizontal channel flows [36]. The two articles of Ambati and Bokhove [51, 52] are among the very few papers that deal with DG methods over dry beds [53, 54]. In their work, the authors presented a second-order DG space–time FE discretization combined with an improvement to the HLLC [4] flux. Space-time elements separate accurately the wet and dry sub-domains by moving the mesh accurately in a transient manner. Newly, Castro and Toro [55] reported an ADER very high-order approach for the shallow water equations in the framework of DG methods. In addition, Kesserwani *et al.* [56] reported the application of a second-order RKDG model (RKDG2) to the full conservative form of the Saint Venant system. The algorithm proved to be effective compared with a traditional TVD-FV model implemented with the same properties as RKDG2, i.e. second-order accuracy, Roe Riemann solver, and straightforward approximations of the source terms integrals. Nevertheless, the proposed model was elaborated for second-order accuracy achievements in space and time.

DOI: 10.1002/fld

We believe that detailing a practical implementation of high-order RKDG models is an issue of feasible interest to open-channel flows modellers. Consequently, we survey a practical high-order RKDG formulation for the computation of hyperbolic conservation laws, particularly the shallow water equations. The scheme is formally fourth-order accurate (RKDG4) with constant, linear, parabolic, and cubic basis functions, representing the cell average and its corresponding high-order slopes of the flow variables in each element. The algorithm was designed in conjunction with the Roe Riemann solver [37] inducted with an entropy fix (so that the method is able to handle transcritical flow transitions without generating forged discontinuous shocks), an adaptive slope limiting procedure (so that the limiting procedure is applied only where it is needed), and high-order approximations of the source terms components. We next advocate the advantages of using the RKDG4 method by comparing its performance with the RKDG2 model [56] discussing the issues of error magnitudes and CPU time cost. Then, we aim at computing, using the RKDG4 method, traditional flow problems with/without source terms effects for a more detailed numerical verification.

This paper is organized as follows. In Section 2, we sketch the 1D open-channel flow mathematical model. Section 3 describes the practical formulation of the RKDG4 scheme. Section 4 exhibits the numerical performance of the proposed RKDG4 via steady and transient benchmark tests.

2. OPEN-CHANNEL FLOW EQUATIONS

The shallow water, or the Saint Venant, equations [5, 6] are accepted for many practical applications as a proper model of unsteady flow of water in 1D space dimension. The equations express the physical conservation principles of mass and momentum. Assuming a gently varying topography, this mathematical model describes the wetted cross-sectional area $A(x,t)$ and the flow discharge $Q(x,t)$ variations in the direction parallel to the bottom (x denotes a coordinate in the horizontal direction and t denotes the time). Based on the hydrostatic pressure distribution and incompressible flow assumptions, the 1D unsteady Saint Venant equations are described as

$$\begin{aligned} &A_t + Q_x = 0 \\ &Q_t + (Q^2/A + gI_1)_x = gA(S_0 - S_f) + gI_2 \end{aligned} \tag{1}$$

where g is the gravity constant, $S_0 = -\partial z/\partial x$ is the bed slope ($z(x)$ represents the bed elevation), and S_f stands for friction forces, with S_f associated with wall friction and may be defined by an empirical law [5, 6] in terms of Manning's roughness coefficient (denoted by n). I_1 and I_2 are integral terms accounting for pressure forces (hydrostatic-pressure and wall-pressure terms, respectively). In the particular case of a symmetrical trapezoidal cross section, $I_1 = bh^2/2 + S_L h^3/3$ and $I_2 = \partial I_1/\partial x|_{h=\text{constant}}$, where $h(x,t)$ describes the height of water, $b(x)$ the width of the channel's bottom, $b'(x)$ its derivative, and S_L the channel's side slope [57], which is null in the case of a rectangular cross section.

Recently developed research codes [8, 9, 11, 12, 14, 15, 17, 56] are based on the conservative formulation of this set of hyperbolic PDE, namely

$$U_t + F(U)_x = G \tag{2}$$

where $U = [A \;\; Q]^T$ designates the flow vector, $F(U) = [Q \;\; Q^2/A + gI_1]^T$ the flux vector, and $G(U) = [0 \;\; gA(S_0 - S_f) + gI_2]^T$ the source term vector.

DOI: 10.1002/fld

By using the Jacobian matrix of the flux ($J=\partial F/\partial U$) with respect to the flow vector, Equation (2) can be further expressed in a quasi-linear form as

$$U_t + JU_x = G \tag{3}$$

J has two real eigenvalues $a^{1,2}=u\pm c$, where $c=\sqrt{gh(b+hS_L)/(b+2hS_L)}$ designates the wave celerity. Moreover, the hyperbolic nature of the equation ensures that matrix J has a complete set of independent and real eigenvectors $e^{1,2}=[1\ \ a^{1,2}]^T$.

In the cases of non-prismatic channels, the total derivative of the flux vector involves, in addition to the partial derivative with respect to the conserved variable (JU_x), a partial derivative with respect to the space variation $\partial F/\partial x$. Therefore, the supplementary partial derivative has been moved to the right-hand side of Equation (2), and the source term vector is redefined as $G=G-\partial F/\partial x$ allowing the passage to an associated non-conservative form (see [8, 9, 58]).

3. HIGH-ORDER RKDG4 MODEL

This section describes the construction and implementation of high-order RKDG methods up to fourth order in space and time for, particularly, the 1D shallow water equations. We present the implementation of the RKDG4 scheme such that lowest-order models may be easily deducted. The computational interval is divided into N uniform cells with boundary points $0=x_{1/2}<x_{3/2}<\cdots<x_{N+1/2}=L$. The points $x_i=(x_{i+1/2}+x_{i-1/2})/2$ are the centers of the cells $I_i=[x_{i-1/2}, x_{i+1/2}]$ and $\Delta x=x_{i+1/2}-x_{i-1/2}$ the cell's size, which is assumed to be uniform. The proposed discretization is considered according to the approach of Cockburn and Shu [34]. We seek a local approximation $U_h=[A_h\ \ Q_h]^T$ to U such that, for each time step $t\in[0,T]$, U_h belongs to the finite-dimensional space $P^k(I_i)$ of polynomial in I_i of degree at most k (achieving $(k+1)$th-order accuracy in space). Hence, system (2) is multiplied by an arbitrary smooth function v_h and integrated over I_i. Subsequently, the flux term is integrated by part to obtain the following weak formulation:

$$\int_{I_i}\partial_t U_h v_h\,dx-\int_{I_i}F(U_h)\partial_x v_h\,dx+[F(U_h)v_h]_{i+1/2}-[F(U_h)v_h]_{i-1/2}=\int_{I_i}G(U_h)v_h\,dx \tag{4}$$

With the aim of decoupling the system, we adopt the Legender polynomials (P_l) as the local basis functions to obtain a diagonal mass matrix. Similarly, in the standard DG we select $\varphi_l^i(x)=P_l(2(x-x_i)/\Delta x)$ as a test function v_h. Since the interest is to design a fourth-order space accuracy scheme, the method was set up for $k=3$, corresponding to piecewise cubic approximations. Therefore, four basis functions $\{\varphi_0^i(x), \varphi_1^i(x), \varphi_2^i(x), \varphi_3^i(x)\}$ are needed:

$$\left\|\begin{array}{l}\varphi_0^i(x)=1\\ \varphi_1^i(x)=2(x-x_i)/\Delta x\\ \varphi_2^i(x)=6(x-x_i)^2/\Delta x^2-1/2\\ \varphi_3^i(x)=20(x-x_i)^3/\Delta x^3-3(x-x_i)/\Delta x\end{array}\right. \tag{5}$$

DOI: 10.1002/fld

and, accordingly, the approximation of the solution $U_{\mathrm{h}}(x,t)$ over each cell I_i is expressed as

$$U_{\mathrm{h}}(x,t)=\sum_{l=0}^{k} U_i^l(t)\varphi_l^i(x) \quad \forall x\in I_i \tag{6}$$

At each time step, one has to solve for the expansion coefficients $U_i^0(t)$, $U_i^1(t)$, $U_i^2(t)$, and $U_i^3(t)$ of the FE approximation, going from the initial condition ($U(x,0)=U_0(x)$) projections, which are defined [34] by

$$U_i^l(0)=(2l+1)/\Delta x\int_{I_i} U_0(x)\varphi_l^i(x)\,\mathrm{d}x, \quad l=0,1,\ldots,k \tag{7}$$

and, for the degrees of freedom update, one has to proceed as follows

$$\mathrm{d}U_i^l/\mathrm{d}t=L_{\mathrm{h}}(U_{\mathrm{h}}) \quad \text{for } l=0,1,2,\ldots,k \tag{8}$$

with

$$L_l(U_{\mathrm{h}})=-(2l+1)/\Delta x\left[\tilde{F}(U_{i+1/2}^-,U_{i+1/2}^+)-(-1)^l\tilde{F}(U_{i-1/2}^-,U_{i-1/2}^+)\right.$$
$$\left.-\int_{x_{i-1/2}}^{x_{i+1/2}} F(U_{\mathrm{h}})(\varphi_l^i(x))_x\,\mathrm{d}x-\int_{x_{i-1/2}}^{x_{i+1/2}} G(U_{\mathrm{h}})\varphi_l^i(x)\,\mathrm{d}x\right] \tag{9}$$

$U_{i+1/2}^{\pm}=U_{\mathrm{h}}(x_{i+1/2}^{\pm},t)$ are the left and right limits of the discontinuous solution U_{h} at the cell's interface and $\tilde{F}(U_{\mathrm{L}},U_{\mathrm{R}})$ is a numerical flux function based on Roe's [37] numerical flux function taking the following form

$$\tilde{F}(U^-,U^+)=0.5\left[F(U^-)+F(U^+)-\sum_{p=1}^{2}\alpha_{\mathrm{int}}^p|\tilde{a}_{\mathrm{int}}^p|\tilde{e}_{\mathrm{int}}^p\right] \tag{10}$$

where the subscript 'int' designates the intermediate state between the left and right states. Once the Roe average velocity and celerity ($\tilde{u}_{\mathrm{int}},\tilde{c}_{\mathrm{int}}$) are found, the mean eigenvalues $\tilde{a}_{\mathrm{int}}^p$ and eigenvector $\tilde{e}_{\mathrm{int}}^p$ are found. An average of pth waves strength α_{int}^p is found by an explicit formula involving U^-, U^+, $\tilde{u}_{\mathrm{int}}$, and $\tilde{c}_{\mathrm{int}}$ (see [14] for clear-cut formulations). Moreover, to avoid having unphysical expansion shocks in the solution [3], the absolute eigenvalues are modified using an entropy fix, namely

$$|\tilde{a}_{\mathrm{int}}^p|^*=\begin{cases}|\tilde{a}_{\mathrm{int}}^p| & \text{if } |\tilde{a}_{\mathrm{int}}^p|\geqslant\varepsilon^p\\ (\tilde{a}_{\mathrm{int}}^p)^2/(2\varepsilon^p)+\varepsilon^p/2 & \text{if } |\tilde{a}_{\mathrm{int}}^p|<\varepsilon^p\end{cases} \tag{11}$$

where

$$\varepsilon^p=\min[\tilde{c}_{\mathrm{int}},\max(0,2((a^p)^+-(a^p)^-))] \tag{12}$$

To avoid the Gibbs phenomenon in the vicinity of strong shocks, we replace $U_{i\pm1/2}^{\pm}$ by the interfacial values of each slope limited [3] cell's approximation (denoted by $\hat{U}_{i\pm1/2}^{\pm}$). As we are dealing with high-order piecewise approximations, an adaptive limiting action (explicitly described) is

DOI: 10.1002/fld

performed by the use of the *generalized minmod* limiter function [28]. It is important both to start limiting from the highest coefficient and to stop when the first coefficient that does not need to be limited is reached. By this means the limiter is applied only where it is needed and retains an order as high as possible and does not automatically reduce to first order. A general comprehensive framework of the moment limiter [39] was recently described by Krivodonova [40]. The limiter is used in the following manner

SET $l=k$

Limit U_i^l by replacing it by $\hat{U}_i^l=\text{minmod}((2l-1)U_i^l, U_{i+1}^{l-1}-U_i^{l-1}, U_i^{l-1}-U_{i-1}^{l-1})/(2l-1)$

If $\hat{U}_i^l=U_i^l$

STOP; $\hat{U}_{i\pm1/2}^{\mp}=\sum_{s=0}^{l}(\pm1)^s U_i^s+\sum_{s=l+1}^{k}(\pm1)^s\hat{U}_i^s$

OTHERWISE

replace $l=l-1$;

continue until $l=1$

In treatment of integral terms of Equations (7) and (9), we used quadrature rules. Here k is the aforementioned order of the approximating polynomial. For Gaussian rules, one requires $(k+1)$-nodes to conserve the accuracy order of the full method. This means that for $l=0,1,2,\ldots,k$ it suffices to use the $(l+1)$-points Gaussian rules, respectively.

For $k=3$, the initial condition projections and the DG space operators are manipulated to be

$$\begin{aligned}
&U_i^0(0)=\bar{U}_i=U_0(x_i)\\
&U_i^1(0)=\sqrt{3}/2[U_0(x_i+\Delta x\sqrt{3}/6)-U_0(x_i-\Delta x\sqrt{3}/6)]\\
&U_i^2(0)=5/9[U_0(x_i-\Delta x\sqrt{15}/10)-2U_0(x_i)+U_0(x_i+\Delta x\sqrt{15}/10)]\\
&U_i^3(0)=7\{\mu\delta(20\delta^2-3)[U_0(x_i+\delta\Delta x)-U_0(x_i-\delta\Delta x)]\\
&\qquad\quad+\mu'\delta'(20\delta'^2-3)[U_0(x_i+\delta'\Delta x)-U_0(x_i-\delta'\Delta x)]\}
\end{aligned}\tag{13}$$

$$\begin{aligned}
L_0(U^0,U^1,U^2,U^3)&=-1/\Delta x[\tilde{F}_{i+1/2}-\tilde{F}_{i-1/2}-S_i^0]\\
L_1(U^0,U^1,U^2,U^3)&=-3/\Delta x[\tilde{F}_{i+1/2}+\tilde{F}_{i-1/2}-F(U_i^0-U_i^1/\sqrt{3})-F(U_i^0+U_i^1/\sqrt{3})-S_i^1]\\
L_2(U^0,U^1,U^2,U^3)&=-5/\Delta x\{\tilde{F}_{i+1/2}-\tilde{F}_{i-1/2}-\sqrt{15}/3[F(U_i^0+U_i^1\sqrt{15}/5+2U_i^2/5)\\
&\qquad-F(U_i^0-U_i^1\sqrt{15}/5+2U_i^2/5)]-S_i^2\}\\
L_3(U^0,U^1,U^2,U^3)&=-7/\Delta x\{\tilde{F}_{i+1/2}+\tilde{F}_{i-1/2}-3\mu(20\delta^2-1)[F(U_{\text{h}}(x_i+\delta\Delta x))\\
&\qquad-F(U_{\text{h}}(x_i-\delta\Delta x))]-3\mu'(20\delta'^2-1)[F(U_{\text{h}}(x_i+\delta'\Delta x))\\
&\qquad-F(U_{\text{h}}(x_i-\delta'\Delta x))]-S_i^3\}
\end{aligned}\tag{14}$$

DOI: 10.1002/fld

where $\tilde{F}_{i\pm1/2}=\tilde{F}(\hat{U}^{-}_{i\pm1/2},\hat{U}^{+}_{i\pm1/2})$, $U_{\mathrm{h}}(x_i\pm\delta\Delta x)=U_i^0\pm2\delta U_i^1+(6\delta^2-1/2)U_i^2\pm\delta(20\delta^2-3)U_i^3$, $\delta=1/2\sqrt{(15+2\sqrt{30})/35}$, $\delta'=1/2\sqrt{(15-2\sqrt{30})/35}$, $\mu=1/4-\sqrt{30}/72$, and $\mu'=1/4+\sqrt{30}/72$. S_i^l $(l=0,1,2,3)$ designate the $(l+1)$th-order source term vector approximations, which are given by

$$\left\|\begin{aligned}
S_i^0 &= G(U_i^0)\\
S_i^1 &= \Delta x\sqrt{3}/6[G(U_i^0+U_i^1/\sqrt{3})-G(U_i^0-U_i^1/\sqrt{3})]\\
S_i^2 &= 5/18[(3\sqrt{15}/5-\Delta x/2)G(U_i^0+U_i^1\sqrt{15}/5+2U_i^2/5)\\
&\quad -(3\sqrt{15}/5+\Delta x/2)G(U_i^0-U_i^1\sqrt{15}/5+2U_i^2/5)]\\
S_i^3 &= \Delta x\{\mu\delta(20\delta^2-1)[G(U_{\mathrm{h}}(x_i+\delta\Delta x))-G(U_{\mathrm{h}}(x_i-\delta\Delta x))]\\
&\quad +\{\mu'\delta'(20\delta'^2-1)[G(U_{\mathrm{h}}(x_i+\delta'\Delta x))-G(U_{\mathrm{h}}(x_i-\delta'\Delta x))]\}
\end{aligned}\right. \tag{15}$$

As a final point, fourth-order accuracy in time is enhanced, to the fourth space order semi-discrete scheme (14), by a four-step nonlinearly stable RK time marching with a CFL [16] number equal to 0.145 for stability requirements [34]. Thus, the updating of the degrees of freedom is performed

$$\left\|\begin{aligned}
(U^{0,1,2,3})^{\mathrm{int1}} &= (U^{0,1,2,3})^n+\Delta t L_{0,1,2,3}((U^0)^n,(U^1)^n,(U^2)^n,(U^3)^n)\\
(U^{0,1,2,3})^{\mathrm{int2}} &= (U^{0,1,2,3})^n+\Delta t/2 L_{0,1,2,3}((U^0)^{\mathrm{int1}},(U^1)^{\mathrm{int1}},(U^2)^{\mathrm{int1}},(U^3)^{\mathrm{int1}})\\
(U^{0,1,2,3})^{\mathrm{int3}} &= (U^{0,1,2,3})^n+\Delta t/2 L_{0,1,2,3}((U^0)^{\mathrm{int2}},(U^1)^{\mathrm{int2}},(U^2)^{\mathrm{int2}},(U^3)^{\mathrm{int2}})\\
(U^{0,1,2,3})^{n+1} &= 1/3[-(U^{0,1,2,3})^n+(U^{0,1,2,3})^{\mathrm{int1}}-2(U^{0,1,2,3})^{\mathrm{int2}}+(U^{0,1,2,3})^{\mathrm{int3}}]\\
&\quad +\Delta t/6 L_{0,1,2,3}((U^0)^{\mathrm{int3}},(U^1)^{\mathrm{int3}},(U^2)^{\mathrm{int3}},(U^3)^{\mathrm{int3}})
\end{aligned}\right. \tag{16}$$

Remark

The RKDG3 model is obtained by removing the variable $U^3(t)$ from the previous formulas (Equations (13) and (14)) and by considering the DG space operators up to second-order (i.e. L_0, L_1, and L_2). Regarding the time discretization, we used a three-step RK stepping with a CFL number equal to 0.209 as follows

$$\left\|\begin{aligned}
(U^{0,1,2})^{\mathrm{int1}} &= (U^{0,1,2})^n+\Delta t L_{0,1,2}((U^0)^n,(U^1)^n,(U^2)^n)\\
(U^{0,1,2})^{\mathrm{int2}} &= 3/4(U^{0,1,2})^n+1/4(U^{0,1,2})^{\mathrm{int1}}+\Delta t/4 L_{0,1,2}((U^0)^{\mathrm{int1}},(U^1)^{\mathrm{int1}},(U^2)^{\mathrm{int1}})\\
(U^{0,1,2})^{n+1} &= 1/3(U^{0,1,2})^n+2/3(U^{0,1,2})^{\mathrm{int2}}+2\Delta t/3 L_{0,1,2}((U^0)^{\mathrm{int2}},(U^1)^{\mathrm{int2}},(U^2)^{\mathrm{int2}})
\end{aligned}\right. \tag{17}$$

4. NUMERICAL TESTS AND RESUTLS

This section analyzes the performance of the described RKDG4 scheme implementation for the simulation of hyperbolic conservation laws, particularly the shallow water equations. We first

DOI: 10.1002/fld

survey a comparison of the RKDG2 model [56] with higher-order models to shift an emphasis of considering the RKDG4 method. We next illustrate the RKDG4 numerical approximation results, when applied to the shallow water equations, by means of steady and transient benchmarks with reference solutions that are used to verify the functioning of the proposed scheme.

4.1. Comparison between the RKDG4 model and lower-order models

4.1.1. Transient Burger's equation. We solve, for this test, the inviscid nonlinear Burger's equation $u_t+(u^2/2)_x=0$. Aiming for an understandable representation of the DG polynomial approximations structure, we firstly consider a case with transitive boundary conditions and a domain $[0, 100]$ with an initial condition leading to a left depression wave and a right shock wave propagations [3]. It is given as follows

$$u_0(x)=\begin{cases}-0.5 & \text{if } 32.5\leqslant x\leqslant 77.5\\ 2 & \text{otherwise}\end{cases} \tag{18}$$

This profile is convected till $T=15\,\text{s}$ and the linear, parabolic, and cubic approximations corresponding to the RKDG2, RKDG3, and RKDG4 models are, respectively, shown in Figure 1. However, in all next numerical tests, only the mean value of the polynomial approximation over each cell will be considered and plotted against an analytical value.

The second case surveys a quantitative comparison between high-order RKDG methods. The smooth initial condition $u_0(x)=0.25+0.5\sin(\pi(2x-1))$ is considered on the domain $[0, 1]$. Periodic boundary conditions are used and the simulation is stopped at a time of $T=0.05\,\text{s}$ before which the compression wave becomes a shock. At a first sight (Figure 2), the advantage of using the RKDG4 model is flagrantly noticed from the magnified left portion of the sine wave. It reflects the usefulness of the RKDG4 model for achieving a better agreement with the exact solution, by using less computational cells, than the RKDG2 scheme. Figure 3 is a plot of the errors with respect to the number of computational cells, while Table I lists quantitatively the errors achieved, respectively, by the RKDG2, RKDG3, and RKDG4 models. The way in which the errors are evaluated is

$$\text{Error}=\frac{1}{N}\frac{\sum_{i=1}^{N}|u(x_i)-(u_i^0)^n|}{\sum_{i=1}^{N}|u(x_i)|} \tag{19}$$

By this means, we note that in terms of CPU time cost the RKDG4 model is almost twice as costly as the RKDG2 model for the same mesh, since two more DG operators are involved for RKDG4 instead of two for RKDG2. On the other hand, the RKDG4 model has generated half the number of the errors that are produced by the RKDG2 scheme, which points up an economical practicability of RKDG4. However, it is worth stressing that if one wants to refine the number of computational cells to more than $N=52$, no serious qualitative difference are noted between the RKDG2 model and higher-order models. Thus, next we present a similar comparison on the Saint Venant system with source terms for $N=52$.

4.1.2. Steady subcritical flow in a trapezoidal conduit. MacDonald [57] and MacDonald *et al.* [59] proposed a series of open-channel flow test cases with analytical solutions. In all of them, sloping bed and friction force are considered. Given a constant discharge, a Manning coefficient,

DOI: 10.1002/fld

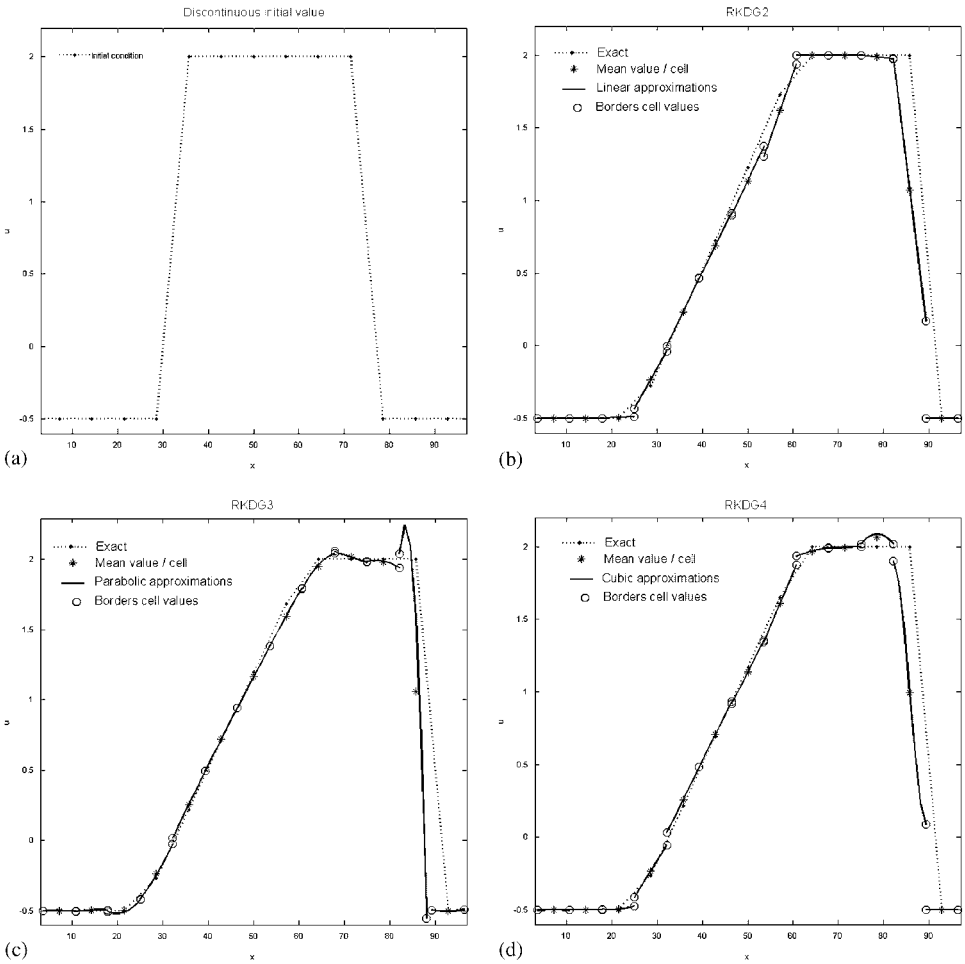

Figure 1. Numerical solutions of the Burger's equation by means of high-order RKDG methods going from a discontinuous initial condition.

and the channel width together with an analytical water depth function, the bed slope is found from the momentum equation of the steady Saint Venant equations

$$S_0 = \left[1 - \frac{Q^2(b+2hS_L)}{g(b+hS_L)^3h^3}\right]h' + \frac{Q^2n^2(b+2h\sqrt{1+S_L})^{4/3}}{[(b+hS_L)h]^{10/3}} - \frac{Q^2hb'}{g(b+hS_L)^3h^3} \tag{20}$$

The example used herein consists of a trapezoidal channel of width $b=10\,\text{m}$, lateral slope $S_L=2$, and length $L=5000\,\text{m}$ with a bed material characterized by a friction Manning coefficient of $n=0.03$ (SI units) and a steady flow discharge of $Q=20\,\text{m}^3/\text{s}$. The free surface, bed and critical level profiles are shown in Figure 4(b), where the analytical steady-state water depth is

DOI: 10.1002/fld

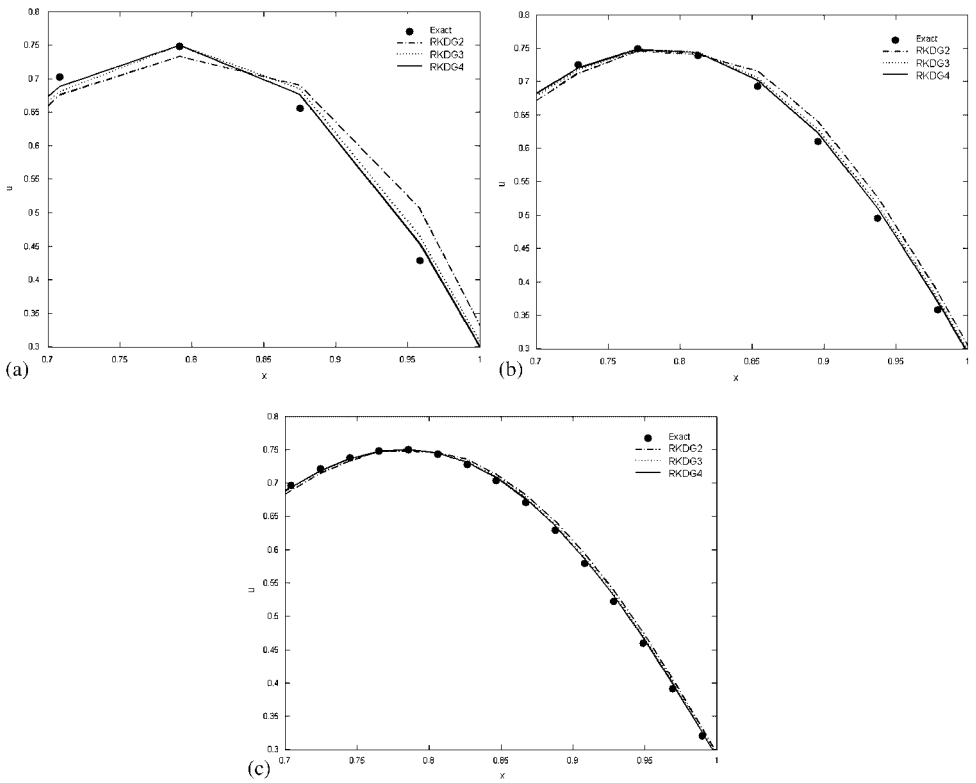

Figure 2. Numerical solutions compared with the exact solution of the Burger's equation going from a smooth initial condition and simulated with high-order RKDG models: (a) $N=13$; (b) $N=26$; and (c) $N=52$.

given by

$$h(x)=9/8+0.25\sin(\pi x/500) \tag{21}$$

The depth solution corresponds to a wholly smooth sinusoidal flow in the channel. The numerical unsteady model is given steady boundary conditions to obtain finally a numerical steady-state solution and compared with the analytical solution (21). Owing to the subcritical nature of the flow, one physical boundary condition has to be enforced at, each, the upstream boundary ($Q=20\,\mathrm{m}^3/\mathrm{s}$) and the downstream boundary ($h=1.1250\,\mathrm{m}$) completed by a numerical boundary condition [58]. $N=52$ computational cells are used for the interval discretization and Figure 5 shows the corresponding numerical depth profiles achieved by the RKDG4 model together with a magnified portion comparing the results of the RKDG2 model with higher-order models. It can be seen that, if one desires to deal with small number of computational cells, the RKDG4 model is able to provide a better agreement with the analytical solution (that was plotted using 200-cell grids). However, as noted in Table II, which summarizes the same as above quantitative errors' comparison on the water depth, the RKDG3 and RKDG4 required, respectively, more than three and nine times the CPU cost of the RKDG2 model.

DOI: 10.1002/fld

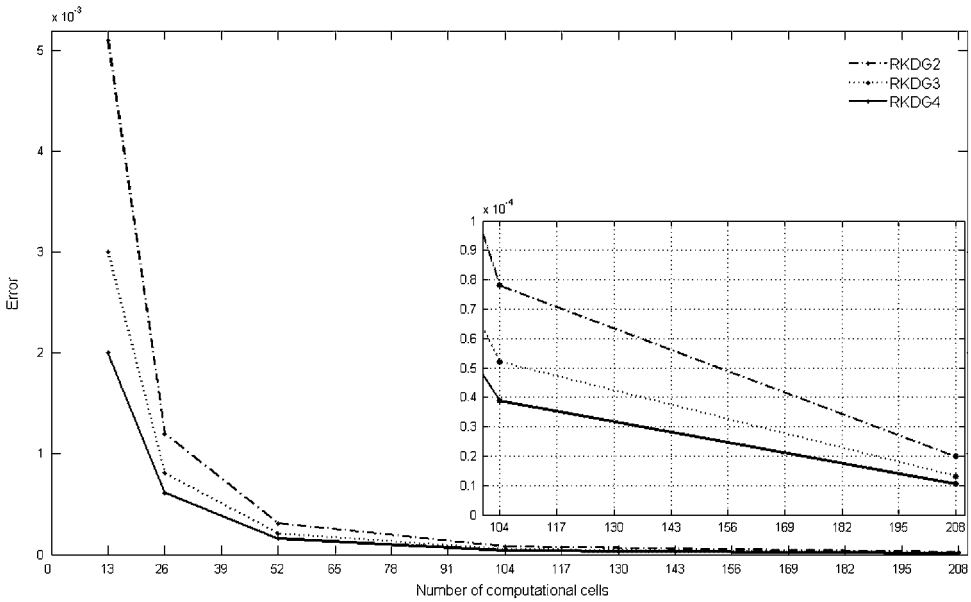

Figure 3. Error evolution with respect to the number of computational cells.

Table I. CPU times and velocity errors generated, respectively, by the RKDG2, RKDG3, and RKDG4 schemes for the transient Burger's equation.

	RKDG2		RKDG3		RKDG4	
N	Error (%)	CPU (s)	Error (%)	CPU (s)	Error (%)	CPU (s)
13	5.1e−001	0.10	3.0e−001	0.13	2.0e−001	0.25
26	1.2e−001	0.14	8.1e−002	0.23	6.1e−002	0.37
52	3.1e−002	0.22	2.0e−002	0.31	1.5e−002	0.68
104	7.8e−003	0.52	5.2e−003	0.79	3.8e−003	1.16

4.2. Application of RKDG4 to supercritical and discontinuous flow benchmarks

So far, in spite of their large CPU time cost, higher than second-order RKDG models are not, in principle, the superlative choice for dealing with realistic discontinuous flows, which explains the pending research on designing their suitable high-order (differentiable) limiter functions. Although knowing that, we focus in this subsection on displaying the RKDG4 model performance when utilized to compute the full conservative form of the shallow water equations.

4.2.1. Steady supercritical flow in a prismatic channel. It is a rectangular prismatic reach 1000 m long and 10 m wide in which the flow is supercritical at the inflow and outflow. In Figure 4(a), the exact longitudinal profiles of water level, critical level, and bottom level are displayed. The

DOI: 10.1002/fld

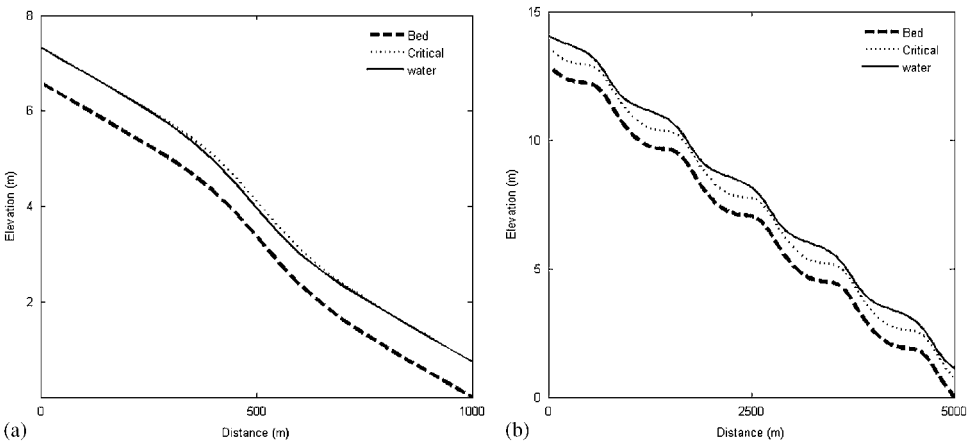

Figure 4. A schematic view of the flow properties for the steady MacDonald test problems: (a) rectangular prismatic channel of Section 4.2.1 and (b) trapezoidal prismatic channel of Section 4.1.2.

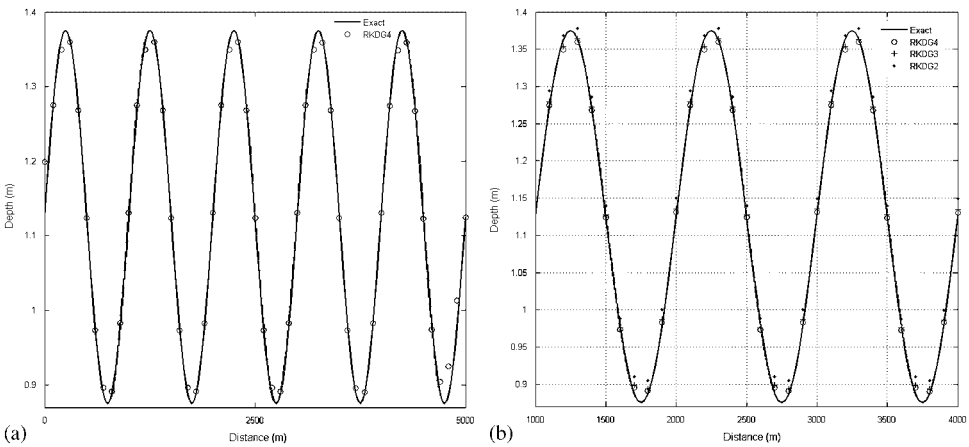

Figure 5. RKDG4 numerical results for the smooth subcritical flow test: (a) along the computational domain and (b) compared with lower-order models on a magnified portion.

discharge is of $20\,\mathrm{m}^3/\mathrm{s}$, the value of the Manning roughness is 0.02 (SI units), and the steady water depth followed

$$h(x)=\left(\frac{4}{g}\right)^{1/3}\left\{1-\frac{1}{5}\exp\left[-36\left(\frac{x}{1000}-\frac{1}{2}\right)^2\right]\right\} \tag{22}$$

Contrary to the downstream boundary, two boundary conditions are enforced at the upstream (a discharge of $20\,\mathrm{m}^3/\mathrm{s}$ is imposed at the upstream boundary and the downstream depth is fixed at 0.741599 m throughout the simulation). Since the flow regime remains unchangeable, $N=13$ computational cells are sufficient for the interval discretization and Figure 6 shows the

DOI: 10.1002/fld

Table II. CPU times and depth errors generated, respectively, by the RKDG2, RKDG3, and RKDG4 schemes for the steady subcritical test.

	RKDG2		RKDG3		RKDG4	
N	Error (%)	CPU (s)	Error (%)	CPU (s)	Error (%)	CPU (s)
13	2.93	6	1.60	13	1.36	40
26	0.47	13	0.30	42	0.28	117
52	3.2e−002	42	1.5e−002	133	1.3e−002	412
104	1.2e−002	149	0.8e−002	513	0.5e−002	1685

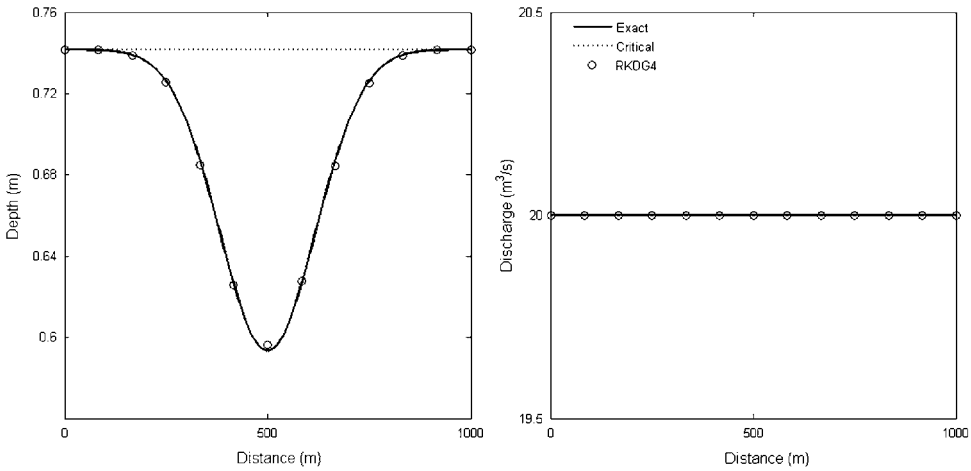

Figure 6. Numerical solution of the supercritical flow test simulated with the RKDG4 scheme versus the exact solution.

corresponding numerical depth and discharge profiles versus the analytical solution (200-cell grids).

4.2.2. Hydraulic jump in a prismatic channel. This is a steady problem of a hydraulic jump modelling in a 1000 m long rectangular prismatic channel of width $b=10$ m with a Manning's roughness coefficient $n=0.02$ and variable bed slope S_0 derived from Equation (20) with the following analytical solution

$$h(x)=\begin{cases}\left(\dfrac{4}{g}\right)^{1/3}\left[\dfrac{9}{10}-\dfrac{1}{6}\exp\left(-\dfrac{x}{250}\right)\right], & 0\leqslant x\leqslant 500\\ \left(\dfrac{4}{g}\right)^{1/3}\left\{1+\displaystyle\sum_{i=1}^{3}k_i\exp\left[-20i\left(\dfrac{x}{1000}-\dfrac{1}{2}\right)\right]\right. & \\ \qquad\left.+\dfrac{1}{2}\exp\left(\dfrac{x}{1000}-1\right)\right\}, & 500<x\leqslant 1000\end{cases} \tag{23}$$

DOI: 10.1002/fld

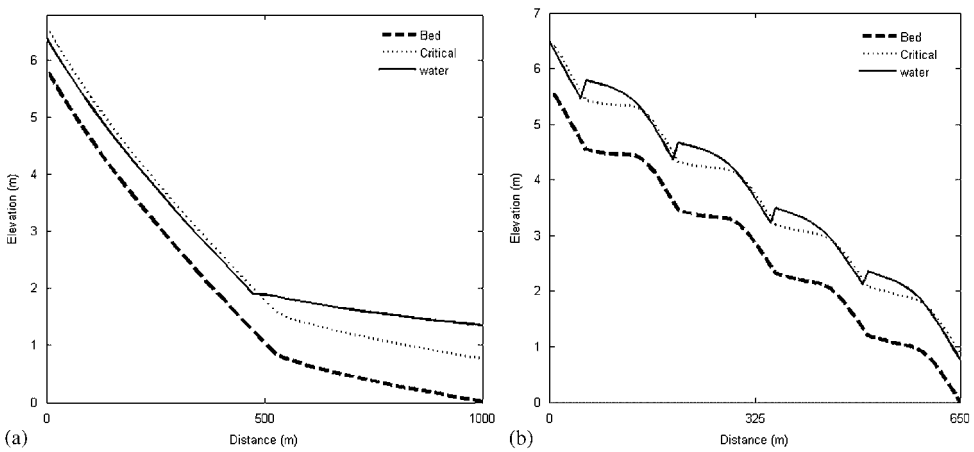

Figure 7. Flow properties of the steady MacDonald test problems of sections: (a) 4.2.2 and (b) 4.2.3.

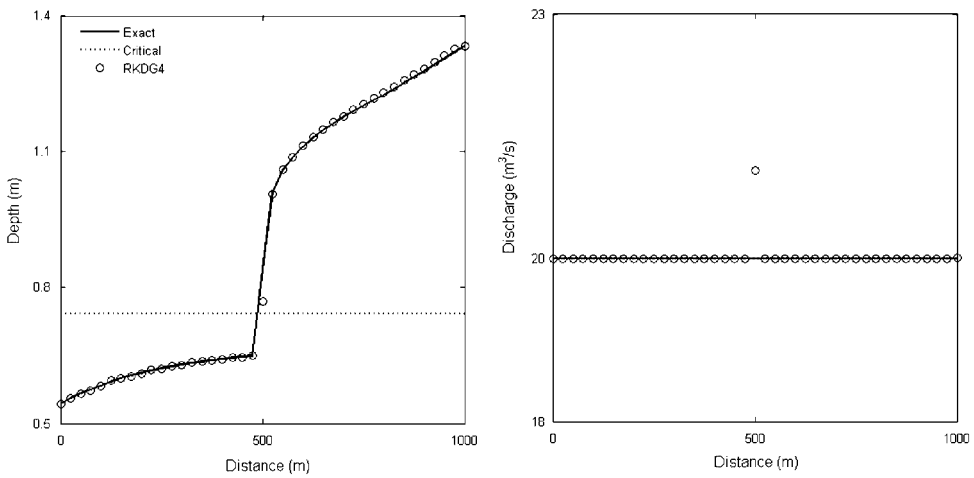

Figure 8. Hydraulic jumps computerized by means of the RKDG4 model and compared with the exact solution.

where $k_1 = -0.348427$, $k_2 = 0.552264$, and $k_3 = -0.555580$. The bed level, water surface level, and critical level longitudinal profiles are illustrated in Figure 7(a). The inflow discharge is $20\,m^3/s$. At this equilibrium state, the flow is supercritical upstream, changes to subcritical halfway along the channel *via* a hydraulic jump occurrence, and remains subcritical thereafter. Therefore, the water depth (0.543853 m) and the water discharge ($20\,m^3/s$) must be prescribed for the upstream boundary conditions. At the downstream end, we specify only one condition (a height of 1.334899 m) as the flow is subcritical and the water discharge is numerically derived [58]. The numerical results using 40 computational cells are adequately reproduced compared with the analytical solution of Figure 8.

DOI: 10.1002/fld

Table III. Analytical solution parameters for Section 4.2.3.

	x_1^*	x_2^*	k_0	k_1	k_2	k_3	a	b	c
$50<x\leqslant 200$	50	200	1.01826	0.0330684	−0.00366582	0.00216754	1	0.25	130
$200<x\leqslant 350$	200	350	1.01031	0.032978	−0.00387227	0.00243084	1	0.23	280
$350<x\leqslant 500$	350	500	0.987768	0.0308504	−0.00416726	0.00294851	0.98	0.2	430
$500<x\leqslant 650$	500	650	0.977391	0.029882	−0.00435568	0.00329588	0.96	0.2	580

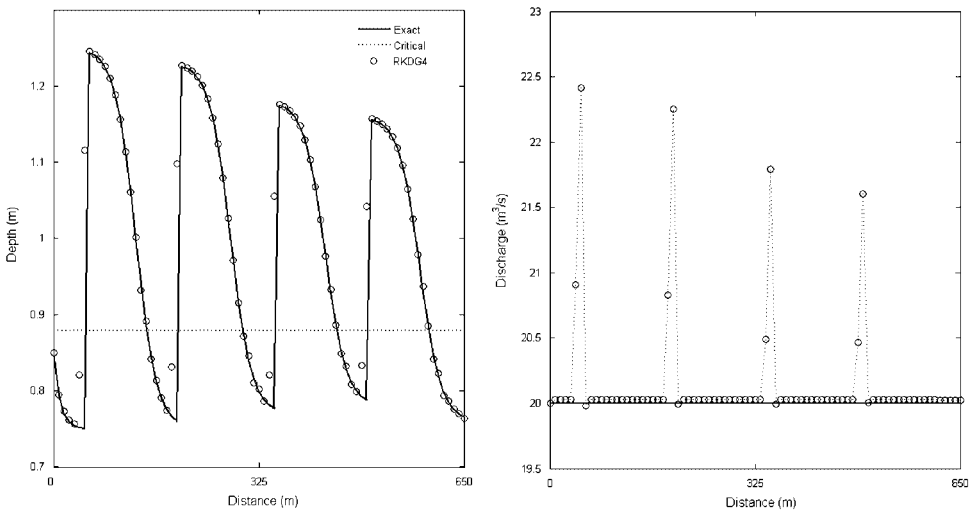

Figure 9. Flow variables profiles computed by means of the RKDG4 model and weighted against the exact solution.

4.2.3. A regression of transcritical flows with shocks in a trapezoidal watercourse. This hydraulic problem consists of a 650m long trapezoidal channel with a roughness coefficient of 0.03. The channel width is $b=5$ m with a lateral slope $S_L=5$. For more understanding of this flow problem, Figure 7(b) contains the bed level and flow properties. The bed slope is calculated from the analytical solution of the depth according to the following equations completed in Table III

$$\begin{aligned} h(x) &= 0.75+0.1\times\exp(0.1x), && x\leqslant 50 \\ h(x) &= \sum_{i=0}^{3} k_i\left(\frac{x-x_1^*}{x_2^*-x_1^*}\right)\times\exp[-50(x-x_1^*)]+a-b\tanh[0.03(x-c)] && \text{otherwise} \end{aligned} \tag{24}$$

The flow is forced to be supercritical at the upstream and the downstream. Two boundary conditions are specified at the upstream ($Q=20\,\mathrm{m}^3/\mathrm{s}$ and $h=0.850$ m) and a free outlet at the downstream.

This example is characterized by a fast variation in the flow regime from supercritical to subcritical generating a succession of stationary shocks and points of transcritical flow. Figure 9 contains the discharge and water depth plots simulated with 81 computational cells. RKDG4 leads to a good approximation of the water stage. The steady discharge prediction is fair, but not ideal as expected [56]. We conjecture that this is because of the high-order adaptive slope limiting

DOI: 10.1002/fld

procedure. It is also worth stressing that the liming procedure, due to the large number of flow discontinuities, led to a huge CPU cost in the simulation of this problem (compared with all the other problems investigated in this essay).

4.2.4. Transcritical flow, with shock, over a hump in a non-prismatic rectangular channel. This is about a steady water flow over a hump in a converging–diverging channel. This kind of flow problem has been largely reported [18, 49, 50, 56] and is characterized by a steady shock formation. The conduit is 3 m long with a smoothly varying bed and width giving the channel a symmetrical form. They are defined as

$$z(x) = \begin{cases} 0.1\cos^2(\pi(x-1.5)) & \text{if } |x-1.5| \leqslant 0.5 \\ 0 & \text{otherwise} \end{cases} \tag{25}$$

$$b(x) = \begin{cases} 1-0.1\cos^2(\pi(x-1.5)) & \text{if } |x-1.5| \leqslant 0.5 \\ 1 & \text{otherwise} \end{cases} \tag{26}$$

Again the flow regime depends on the boundary conditions. Our test case here is that of a transcritical flow with a stationary shock downstream of the hump and a critical point at the throat. The flow is subcritical upstream, turns supercritical in the middle of the channel, and then returns to subcritical downstream passing through a shock. The initial condition is $h+z=1\,\text{m}$ and $Q=1.8796\,\text{m}^3/\text{s}$. Since the flow regime is subcritical at the inflow and the outflow, a single boundary condition should be specified at the upstream and at the downstream. For the upstream boundary condition we impose the water discharge ($Q=1.8796\,\text{m}^3/\text{s}$) and the water depth is calculated numerically. For the downstream boundary, a water depth of 1 m is imposed and the water discharge is taken into account by a numerical boundary condition treatment. An analytical solution can be calculated for each point in the channel by solving a cubic equation that derives from the conservation of water energy [5]. The scheme has been left to convergence and the computerized steady-state profile of the flow variables (with 40 computational cells) compared with the exact solution is shown in Figure 10, where the RKDG4 scheme spots reasonable agreement.

4.2.5. Classical dam-break problem. This test case has become a classical benchmark considered for comparing the performance of numerical schemes specially designed for discontinuous transient flow. Although defined by the system of homogeneous shallow water equations ($G=0$), it is widely considered as a standard test case for validation of schemes. Starting from the initial conditions given by still water and two different water layers separated by a barrier, the theory of characteristics supplies an exact evolution solution that can be used as a reference [60]. At time $T=0$, the barrier is suddenly removed and the corresponding flow pattern consists of a bore travelling downstream and a rarefaction wave travelling upstream. The frictionless channel is 10 m wide and 2000 m length with a flat-bottomed surface. The water depth ratio is $h_d/h_u=0.25$, where $h_u=20\,\text{m}$ is the upstream depth and $h_d=5\,\text{m}$ is the downstream depth. These conditions produce a transcritical flow profile, which means that the flow is subcritical upstream and supercritical downstream. The flow conditions are computed to time $T=50\,\text{s}$. Since the flow up to 50 s does not reach the boundaries, transitive boundary conditions are applied for the upstream and downstream borders. In the simulation, the space interval of the mesh is $\Delta x=20\,\text{m}$ and the RKDG4 results

DOI: 10.1002/fld

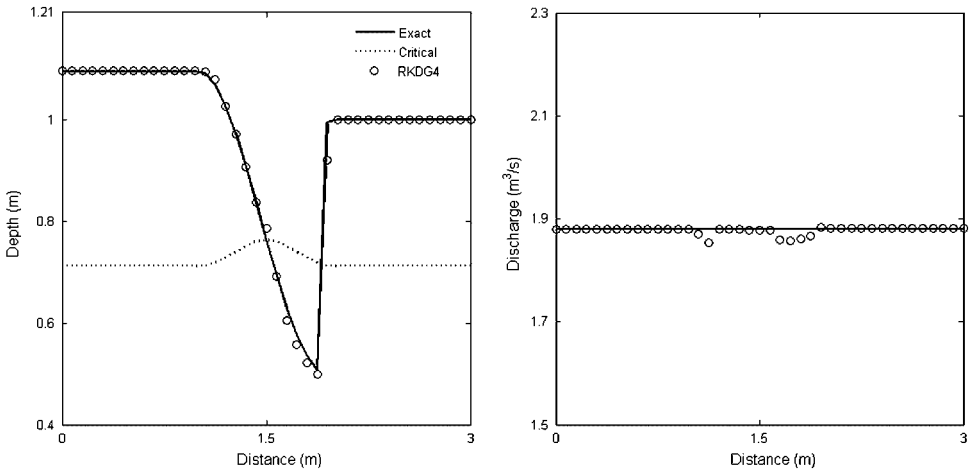

Figure 10. Steady-state profile of the RKDG4 numerics compared with the reference solution.

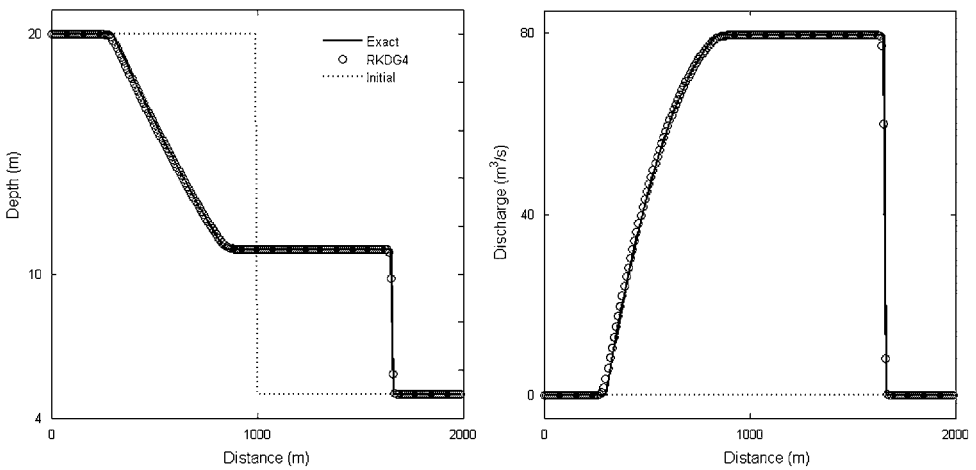

Figure 11. Depth and discharge numerical plots simulated at $T = 50$ s by the RKDG4 scheme.

are illustrated in Figure 11 along with the reference solution showing excellent agreement, where good captures of the discontinuities evolution were handled by the advised scheme.

5. CONCLUSIONS

The shallow water equations not only serve as a set of governing equations for large-scale water waves where the wave amplitude is quite small compared with the wavelength but also provide a good mathematical model for nonlinear hyperbolic differential equations that may have solutions

DOI: 10.1002/fld

such as shock wave and expansion fan. Moreover, solving numerically the shallow water equations is of practical importance for river hydraulics and coastal engineering.

The RKDG model is an evolving class of FE methods that, over the past few years, have dealt with a wide range of problems of practical concern. Contrary to FV techniques, the DG method can lend itself to high-order extensions without the involvement of data reconstructions. Furthermore, this technique has the desirable skill of communicating with only the neighboring data regardless of the accuracy order of the method and uses the interesting properties of well-designed FV shock capturing methods.

To the best of our knowledge, implementation of RKDG techniques to simulate 1D open-channel flows has seen a little formal attention that mostly combines the LLF flux and the HLL family of Riemann solvers. Most recently, a practical implementation of the RKDG2 model gathered with the Roe solver has been constructed and some recent work in applying RKDG models together with the flooding and drying technique has been done for the 1D/2D shallow water model. However, these recent approaches have been designed for second-order accuracy approximations.

In this work, we enabled high-order extensions of the RKDG2 model. The RKDG4 scheme, combined with the Roe solver, was reformulated with high-order source term approximations and an adaptive slope limiting approach. Lately, as a primary step, a comparison between the RKDG4 and lower-order models was carried out indicating the merit of considering the proposed scheme. Finally, the RKDG4 model was applied to simulate steady and transient shallow water flow problems involving mostly discontinuous flow. The computational results were illustrated, together with an available analytical solution, showing the effectiveness and the reliability of the proposed scheme. In principle, only the 1D case is considered in this paper. More work is needed to carry out the detailed design of a well-balanced RKDG (at least for RKDG2 to be later used for practical interests) model over irregular bed topography and this is left for future research.

REFERENCES

1. Guinot V. *Godunov-type Schemes*: *An Introduction for Engineers*. Elsevier: Amsterdam, 2003.
2. Guinot V. *Wave Propagation in Fluids*: *Models and Numerical Techniques*. Wiley: Chichester, England, New York, 2008.
3. Hirsch C. *Numerical Computation of Internal and External Flows*, *Computational Methods for Inviscid and Viscous Flows*. Wiley: Chichester, England, New York, 1990.
4. Toro EF. *Shock-capturing Methods for Free-surface Shallow Flows*. Chichester, England, New York, 2001.
5. Chow VT. *Open-channel Hydraulics*. McGraw-Hill: New York, 1959.
6. Cunge JA, Holly FM, Verwey A. *Practical Aspects of Computational River Hydraulics*. Pitman: London, 1980.
7. van Leer B. Upwind and high-resolution methods for compressible flow: from donor cell to residual-distribution schemes. *Communications in Computational Physics* 2006; **1**(2):192–206.
8. Toro EF, García-Navarro P. Godunov-type methods for free-surface shallow flows: a review. *Journal of Hydraulic Research* 2007; **45**(6):737–751.
9. Burguete J, García-Navarro P. Efficient construction of high-resolution TVD conservative schemes for equations with source terms: application to shallow water flows. *International Journal for Numerical Methods in Fluids* 2001; **37**(2):209–248.
10. Hsu CT, Yeh KC. Iterative explicit simulation of 1D surges and dam-break flows. *International Journal for Numerical Methods in Fluids* 2002; **38**(7):647–675.
11. Delis AI, Katsaounis Th. Relaxation schemes for the shallow water equations. *International Journal for Numerical Methods in Fluids* 2003; **41**(7):695–719.
12. Črnjarić-Žic N, Vuković S, Sopta L. Balanced finite volume WENO and central WENO schemes for the shallow water and the open-channel flow equations. *Journal of Computational Physics* 2004; **200**(2):512–548.
13. Liang Q, Borthwick AGL, Stelling G. Simulation of dam- and dyke-break hydrodynamics on dynamically adaptive quadtree grids. *International Journal for Numerical Methods in Fluids* 2004; **46**(2):127–162.

DOI: 10.1002/fld

14. Crossley AJ, Wright NG. Time accurate local time stepping for the unsteady shallow water equations. *International Journal for Numerical Methods in Fluids* 2005; **48**(7):775–799.
15. Murillo J, García-Navarro P, Brufau P, Burguete J. Extension of an explicit finite volume method to large time steps (CFL>1): application to shallow water flows. *International Journal for Numerical Methods in Fluids* 2006; **50**(1):63–102.
16. Courant R, Friedrichs KO, Lewy H. Über die partiellen differenzangleichungen der mathematisches. *Mathematische Annalen* 1928; **100**(1):32–74.
17. Mohammadian A, Le Roux DY, Tajrishi M. A conservative extension of the method of characteristics for 1-D shallow flows. *Applied Mathematical Modelling* 2007; **31**(2):332–348.
18. Vignoli G, Titarev VA, Toro EF. ADER schemes for the shallow water equations in channel with irregular bottom elevation. *Journal of Computational Physics* 2008; **227**(4):2463–2480.
19. Toro EF, Titarev VA. Derivative Riemann solvers for systems of conservation laws and ADER Methods. *Journal of Computational Physics* 2006; **212**(1):150–165.
20. Godunov SK. Finite difference methods for the computation of discontinuous solutions of the equations of fluid dynamics. *Matematicheskii Sbornik* 1959; **47**(3):271–306.
21. Zhou T, Li Y, Shu CW. Numerical comparison of WENO finite volume and Runge–Kutta discontinuous Galerkin methods. *Journal of Scientific Computing* 2001; **16**(2):145–171.
22. Lax PD. Weak solutions of nonlinear hyperbolic equations and their numerical computation. *Communications of Pure and Applied Mathematics* 1954; **7**(1):159–193.
23. Harten A. High resolution schemes for hyperbolic conservation laws. *Journal of Computational Physics* 1983; **49**(3):357–393.
24. Kurganov A, Tadmor E. New high-resolution central schemes for nonlinear conservation laws and convection–diffusion equations. *Journal of Computational Physics* 2000; **160**(1):241–282.
25. Boris JP, Book DL. Flux corrected transport I, SHASTA, a fluid transport algorithm that works. *Journal of Computational Physics* 1973; **11**(1):38–69.
26. Colella P, Woodward P. The piecewise parabolic method (PPM) for gas-dynamical simulation. *Journal of Computational Physics* 1984; **54**(1):174–201.
27. Harten A, Engquist B, Osher S, Chakravarthy SR. Uniformly high order accuracy essentially non-oscillatory schemes III. *Journal of Computational Physics* 1987; **71**(2):231–303.
28. Harten A, Osher S. Uniformly high-order accurate nonoscillatory schemes I. *SIAM Journal on Numerical Analysis* 1987; **24**(2):279–309.
29. Liu XD, Osher S. Chan T. Weighted essentially non-oscillatory schemes. *Journal of Computational Physics* 1994; **115**(1):408–463.
30. Osher S. Convergence of generalized MUSCL schemes. *SIAM Journal on Numerical Analysis* 1984; **22**(5): 947–961.
31. Shu CW, Osher S. Efficient implementation of essentially non-oscillatory shock capturing schemes. *Journal of Computational Physics* 1988; **77**(2):439–471.
32. Sweby PK. High resolution schemes using flux limiters for hyperbolic conservation laws. *SIAM Journal on Numerical Analysis* 1984; **21**(5):995–1011.
33. van Leer B. Towards the ultimate conservative difference scheme II. Monotonicity and conservation combined in a second order scheme. *Journal of Computational Physics* 1974; **14**(4):361–370.
34. Cockburn B, Shu CW. Runge–Kutta discontinuous Galerkin method for convection-dominated problems. *Journal of Scientific Computing* 2001; **16**(3):173–261.
35. Cockburn B. Discontinuous Galerkin methods. *Zeitschrift für Angewandte Mathematik und Mechanik* 2003; **83**(11):731–754.
36. Kesserwani G, Ghostine R, Vazquez J, Ghenaim A, Mosé R. Riemann solvers with Runge–Kutta discontinuous Galerkin schemes for the 1D shallow water equations. *Journal of Hydraulic Engineering* 2008; **134**(2):243–255.
37. Roe PL, Pike J. Efficient construction and utilization of approximate Riemann solutions. In *Proceedings of Computing Methods in Applied Science and Engineering*, Glowinski R, Lions JL (eds). North-Holland: Amsterdam, 1984.
38. Toro EF. Riemann problems and the WAF method for solving the two dimensional shallow water equations. *Philosophical Transactions of the Royal Society of London* 1992; **338**(1649):43–68.
39. Biswas R, Devine KD, Flaherty J. Parallel, adaptive finite element methods for conservation laws. *Applied Numerical Mathematics* 1994; **14**(1–3):255–283.
40. Krivodonova L. Limiters for high-order discontinuous Galerkin methods. *Journal of Computational Physics* 2007; **226**(1):276–296.

DOI: 10.1002/fld

41. Zhang M, Shu CW. An analysis of and a comparison between the discontinuous Galerkin and the spectral finite volume methods. *Computers and Fluids* 2005; **34**(4–5):581–592.
42. Reed W, Hill T. Triangular mesh methods for the neutron transport equation. *Technical Report LA-UR-73-479*, Los Alamos Scientific Laboratory, Los Alamos, NM, 1973.
43. Schwanenberg D, Kongeter J. A discontinuous Galerkin method for the shallow water equations with source terms. In *Discontinuous Galerkin Methods*, Cockburn B, Karniadakis G, Shu CW (eds). Lecture Notes in Computational Science and Engineering, vol. 11. Springer: Berlin, 2000; 419–424.
44. Babuska I. The p- and hp-versions of the finite element method *The State of the Art. Finite Elements*: *Theory and Applications*. Springer: New York, 1988.
45. Liu Y, Shu C-W, Tadmor E, Zhang M. Central discontinuous Galerkin methods on overlapping cells with a nonoscillatory hierarchical reconstruction. *SIAM Journal on Numerical Analysis* 2007; **45**(6):2442–2467.
46. Nessyahu H, Tadmor E. Non-oscillatory central differencing for hyperbolic conservation laws. *Journal of Computational Physics* 1990; **87**(2):408–463.
47. Dumbser M, Munz CD. Building blocks for arbitrary high order discontinuous Galerkin schemes. *Journal of Scientific Computing* 2006; **27**(1–3):215–230.
48. Dumbser M, Munz CD. ADER discontinuous Galerkin for aeroacoustics. *Comptes Rendus Mécanique* 2005; **333**(9):683–687.
49. Schwanenberg D. Die Runge–Kutta-Discontinuous-Galerkin-Methode zur Lösung konvektionsdominierter tiefengemittelter Flachwasserprobleme. *Ph.D. Thesis*, Fakultät für Bauingenieurwesen, 2003.
50. Xing Y, Shu CW. High order well-balanced finite volume WENO schemes and discontinuous Galerkin methods for a class of hyperbolic systems with source terms. *Journal of Computational Physics* 2006; **14**(2):567–598.
51. Bokhove O. Flooding and drying in discontinuous Galerkin finite-element discretizations of shallow-water equations. Part I: one dimension. *Journal of Scientific Computing* 2005; **22–23**:47–82.
52. Ambati VR, Bokhove O. Space–time discontinuous Galerkin finite element method for shallow water flows. *Journal of Computational and Applied Mathematics* 2006; **204**(2):452–462.
53. Bunya S, Westerink J, Kubatko E, Dawson C. A new wetting and drying algorithm for discontinuous Galerkin solutions to the shallow water equations. *World Congress on Computational Mechanics*, vol. 7, Los Angeles, U.S.A., 2006.
54. Ern A, Piperno S, Djadel K. A well-balanced Runge–Kutta Discontinuous Galerkin method for the shallow-water equations with flooding and drying. *International Journal for Numerical Methods in Fluids* 2008; DOI: 10.1002/fld.1674.
55. Castro CE, Toro EF. ADER DG and FV schemes for shallow water flows. *Fourteenth European Conference on Mathematics for Industry*, *ECMI 2006*, Madrid, Spain, 2006.
56. Kesserwani G, Ghostine R, Vazquez J, Ghenaim A, Mosé R. Application of a second order Runge–Kutta discontinuous Galerkin scheme for the shallow water equations with source terms. *International Journal for Numerical Methods in Fluids* 2008; **56**(7):805–821.
57. MacDonald I. Analysis and computation of steady open channel flow. *Ph.D. Thesis*, University of Reading, 1996.
58. Burguete J, García-Navarro P, Murillo J. Numerical boundary conditions for globally mass conservative methods to solve the shallow water equations and applied to river flow. *International Journal for Numerical Methods in Fluids* 2006; **51**(6):585–675.
59. MacDonald I, Baines MJ, Nichols NK, Samuels PG. Analytical benchmark solutions for open-channel flows. *Journal of Hydraulic Engineering* 1997; **123**(11):1041–1045.
60. Stoker J. *Water Waves*: *The Mathematical Theory with Applications*. Interscience: New York, 1957.